UV Raman Determination of the Environment and Solvent Exposure of Tyr and Trp Residues

Zhenhuan Chi and Sanford A. Asher*

Department of Chemistry, Chevron Science Center, University of Pittsburgh, Pittsburgh, Pennsylvania 15260

Received: June 30, 1998; In Final Form: September 9, 1998

We characterized the dependence of the 229 nm Raman cross sections of tyr and trp on solvent exposure in native horse and tuna cytochrome *c* and in horse and sperm whale myoglobin. Tyr and trp residues with larger solvent accessible surface areas have smaller 229 nm excited tyr and trp Raman cross sections. We observe that in water−propanol solvent mixtures the 229 nm excited tyr and trp Raman cross sections increase with decreasing water composition due to red shifts of the ∼220 nm tyr and trp absorption bands. The tyr and trp protein Raman cross section changes result from absorption red shifts for environments with increasing hydrogen bond donor basicity, decreasing hydrogen bond acceptor acidity, and increasing polarity. We empirically correlate changes in Raman cross sections with the tyr and trp residue solvent accessibility. The Raman cross sections of tyr and trp residues can now be quantitatively utilized to probe local protein environments.

Introduction

An increased understanding of protein structure and function requires the development of better probes of protein structure and amino acid environments.[1−10] In the work here, we characterize the environmental dependence of the UV resonance Raman cross sections of tyr and trp residues. Our study demonstrates that the Raman cross sections of tyr and trp depend sensitively on the nature of the surrounding amino acid side chains and exposure of tyr and trp to water. Thus, UV Raman measurements of tyr and trp can be used as local probes of protein structure. We demonstrate that these cross sections are most sensitive to the water solvent accessibility of the tyr and trp residues.

This new methodology has a significant advantage over the classical techniques for probing tyr and trp structure and dynamics. For example, although UV absorption,[11−13] circular dichroism,[14] and UV fluorescence[15] can measure the tyr and trp spectra, it is very difficult to separate the spectral contributions from different aromatic amino acids. Resonance Raman spectra of tyr and trp show numerous narrow bands, which can be deconvolved to separately distinguish the contributions of different residues.[16−20] In addition, for cases where it is difficult to deconvolute the spectra, it is possible to incorporate isotopic substitutions that separate the spectral contributions.[21]

Experimental Section

Tuna cytochrome *c* (t-cyt), horse heart cytochrome *c* (h-cyt), horse heart myoglobin (h-Mb), cresol, skatole, tyr, trp, *N*-acetyltyrosine ethyl ester (ac-tyr-ee), and *N*-acetyltryptophan ethyl ester (ac-trp-ee) were purchased from Sigma Chemical Co. (St. Louis, MO) and used as received. Sperm whale myoglobin (sw-mb) was generously provided by Drs. Kevin Willis and Arthur Szabo. The heme irons in the cytochrome *c* and myoglobin were in their ferric oxidation state. Methanol, hexanol, 1-propanol, heptane, trifluroethanol (TFE), ether, and acetonitrile were purchased from Aldrich Chemical Co. (Milwaukee, WI). Acetic acid was purchased from Mallinckrodt (Phillipsburg, NJ).

The absolute Raman cross sections of the 932 cm^{-1} band of perchlorate and the 2249 cm^{-1} band of acetonitrile, previously determined by Dudik et al.,[22] were used to calculate the Raman cross sections of tyr and trp. Sodium perchlorate (0.15 M) was used as the internal standard in the aqueous solution samples, while acetonitrile (0.90 M) was used as the internal standard in the water−propanol solvent mixture samples. Raman cross sections were determined by peak height measurements.

UV Raman measurements were obtained by using instrumentation described in detail previously.[20,23] The 229 nm (7 mW) CW laser excitation was obtained from an intracavity frequency-doubled Ar ion laser.[24,25] We used a wire-guided jet sampling system similar to that of Cho et al. to avoid photoaggregation.[19] The spectra were detected by an intensified charge coupled detector (1024 × 256 pixels, Princeton Instruments, Princeton, NJ) with a total accumulation time of 20 min. An 1800 groove/mm grating was used in second order. The spectral resolution was 8.5 cm^{-1} for 229 nm excitation. Absorption spectra were measured by using a Perkin-Elmer Lambda-9 spectrometer.

Results

Figure 1 shows the absorption spectra of ac-trp-ee in water−propanol solvent mixtures. The absorption spectra show a strong ∼220 nm band, which derives from the trp $\pi-\pi^*$ electronic transition to the B_b state, and two overlapping ∼282 and ∼290 nm bands, which derive from the trp $\pi-\pi^*$ electronic transitions to the L_a and L_b states, respectively. When the water concentration decreases, all of the absorption bands systematically red shift, with little band shape change. The B_b band red shifts by 2.7 nm, as the water concentration decreases from 100% to 0%. The inset in Figure 1 displays the linear

* Corresponding author.

10.1021/jp9828336 CCC: $15.00
Published on Web 10/28/1998

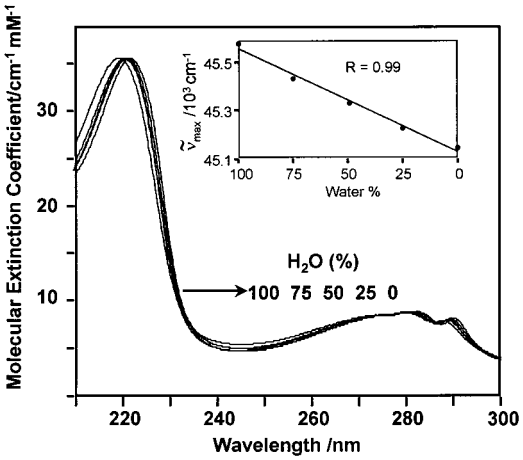

Figure 1. Absorption spectra of ac-trp-ee in different water−propanol solvent mixtures with water concentrations of 100%, 75%, 50%, 25%, and 0% for ac-trp-ee concentrations of 0.33, 0.22, 0.43, 0.65, and 0.86 mM, respectively.

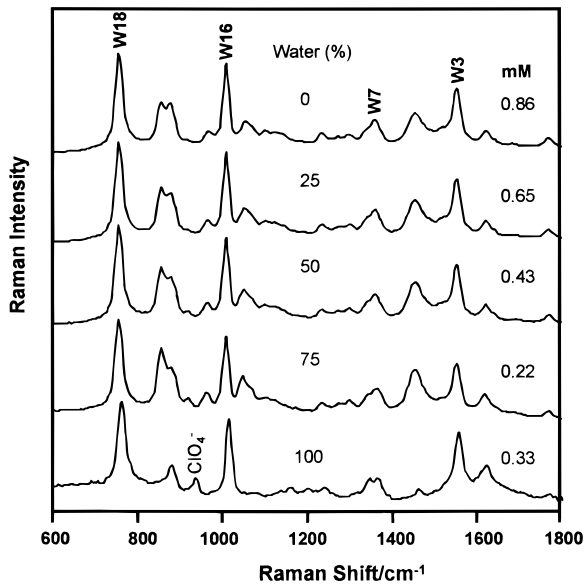

Figure 2. The 229 nm excited resonance Raman spectra of ac-trp-ee in different water−propanol solvent mixtures with water concentrations 100%, 75%, 50%, 25%, and 0% for ac-trp-ee concentrations of 0.33, 0.22, 0.43, 0.65, and 0.86 mM, respectively.

correlation between the B_b band maxima frequency and the water composition (linear correlation coefficient = 0.99).

Figure 2 shows the dependence of the 229 nm resonance Raman spectra of ac-trp-ee on the water−propanol solvent composition. The 855, 885, 964, 1051, and 1455 cm^{-1} bands derive from propanol. The 932 cm^{-1} band in the 100% water spectrum derives from the internal intensity standard perchlorate stretching band. The frequencies and band shapes of the trp bands remain relatively constant, while the intensities increase, as the solvent changes from pure water to pure propanol. Figure 3, which plots the 229 nm excited trp Raman cross section dependence on water concentration, indicates that the Raman cross sections monotonically increase as the water concentration decreases. All of the trp band Raman cross sections in pure propanol are approximately 2-fold larger than those in pure water.

Figure 4 shows the absorption spectra of ac-tyr-ee in water−propanol solvent mixtures. The absorption spectra show a strong band at ~225 nm, which derives from the tyr L_b $\pi-\pi^*$ electronic transition, and a band at ~275 nm, which derives

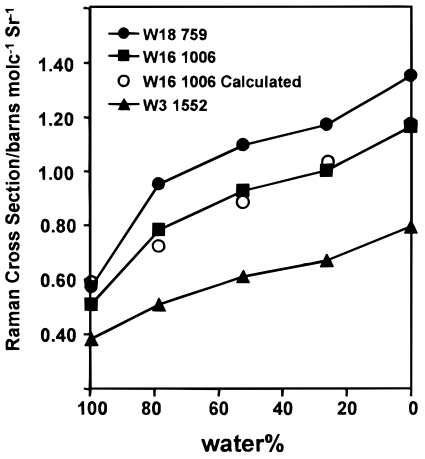

Figure 3. Solvent composition dependence of the 229 nm excited trp band Raman cross sections. The open circles display the calculated cross sections for the 1006 cm^{-1} W16 band.

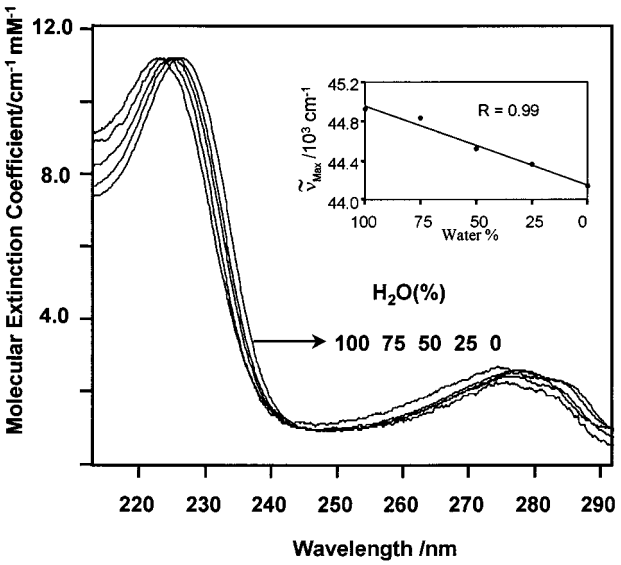

Figure 4. Absorption spectra of ac-tyr-ee in different water−propanol solvent mixtures with water concentrations of 100%, 75%, 50%, 25%, and 0% for ac-tyr-ee concentrations of 0.23, 0.26, 0.52, 0.77, and 1.07 mM, respectively.

from the tyr L_a $\pi-\pi^*$ electronic transition. As the water concentration decreases, all the absorption bands systematically red shift without showing significant band shape changes. The B_b band red shifts by 4.0 nm between 100% and 0% water. The inset in Figure 4 shows a linear correlation between the L_b band maxima and the water composition (linear correlation coefficient = 0.99).

Figure 5 shows the 229 nm excited Raman spectra of ac-tyr-ee in water−propanol solvent mixtures. The 1178, 1208, and 1613 cm^{-1} bands derive from tyr. The Raman cross sections of the tyr bands increase as the water concentration decreases, as shown in Figure 6, which plots the 229 nm excited tyr Raman cross section dependence on the water concentration. The tyr band Raman cross sections monotonically increase as the water concentration decreases. The tyr Raman cross sections in pure propanol are approximately 40% larger than those in pure water.

To further characterize the dependence of the electronic transitions of tyr and trp on environment, we extensively examined the absorption spectra of cresol and skatole in the solvents methanol, propanol, hexanol, acetonitrile, TFE, ethyl ether, acetic acid, and heptane. The positions of the solute

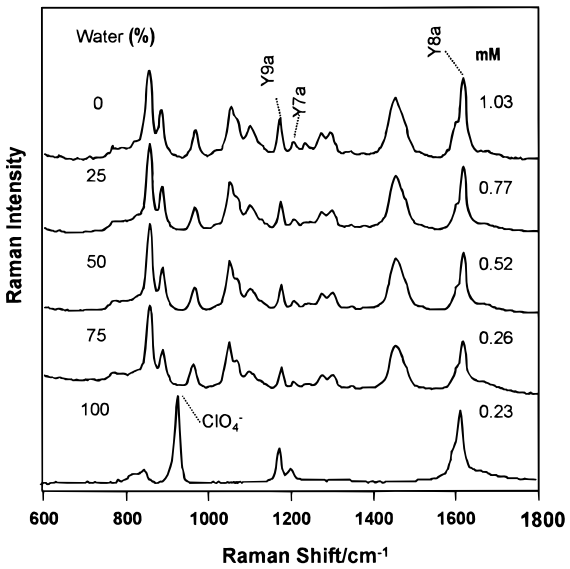

Figure 5. The 229 nm excited resonance Raman spectra of ac-tyr-ee in different water−propanol solvent mixtures with water concentrations of 100%, 75%, 50%, 25%, and 0% for ac-tyr-ee concentrations of 0.23, 0.26, 0.52, 0.77, and 1.07 mM, respectively.

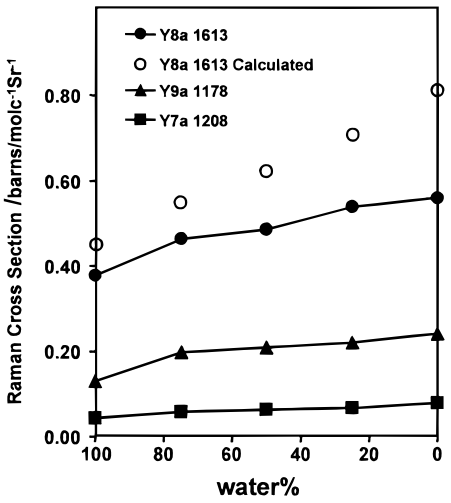

Figure 6. Solvent composition dependence of 229 nm excited tyr band Raman cross sections. The open circles display the calculated cross sections for the 1613 cm^{-1} Y8a band.

absorption band maxima depend on solvent composition. Kamlet, Taft, and co-workers have shown that the solvent dependence can be parametrized by three solvatochromic parameters.[26] The solvent π^* scale is a measure of solvent polarity and polarizability, the α-scale is an index of the solvent hydrogen bond donor acidity, and the β-scale is an index of the solvent hydrogen bond acceptor basicity. These parameters enter linearly into Kamlet−Taft solvatochromic equation:

$$XYZ = XYZ_0 + s\pi^* + a\alpha + b\beta \qquad (1)$$

where XYZ represents a spectral parameter such as the frequency of an absorption spectral maximum and XYZ_0, *s*, *a*, and *b* are the coefficients determined by a multiple linear regression analysis of this spectroscopic parameter for the chromophore under study in different solvents.

Table 1 lists the wavelength and frequency for the absorption maxima of skatole and cresol in these solvents and the calculated solvatochromic parameters (π^*, α, β scales) determined from the absorption spectra.

For skatole

$$\tilde{\nu} = 45169 - 166\pi^* + 175\alpha - 644\beta \qquad (2)$$

with a correlation coefficient of 0.91.

For cresol

$$\tilde{\nu} = 45138 - 105\pi^* + 360\alpha - 846\beta \qquad (3)$$

with a correlation coefficient of 0.87.

Equations 2 and 3 show that the absorption frequency maxima of the ~220 nm absorption bands of skatole and cresol depend on solvent polarity, hydrogen bond donor acidity, and hydrogen bond acceptor basicity. The magnitude of coefficients *s*, *a*, and *b* indicates the strength of interactions between the solvent and skatole and cresol. The fact that coefficient *b* is larger than coefficient *a* indicates that skatole and cresol act more like hydrogen bond donors than hydrogen bond acceptors in these solvents.

The intercepts (45 168 cm^{-1} for skatole and 45 138 cm^{-1} for cresol) represent the absorption maxima of skatole and cresol dissolved in an ideal inert solvent with zero polarity, zero hydrogen bond donor acidity, and zero acceptor basicity. The ideal inert solvent in this case is considered to act as a hard-sphere liquid without interactions with solute molecules.

Figure 7 shows the 229 nm excited resonance Raman spectrum of t-cyt (solid line) and h-cyt (dashed line) and their difference spectrum obtained by subtracting the h-cyt Raman spectrum from the t-cyt Raman spectrum. The 759, 879, 1006, 1178, 1208, 1339, 1359, 1555, and 1613 cm^{-1} bands, which dominate the t-cyt and h-cyt 229 nm excited Raman spectra, derive from tyr and trp. The 759, 879, 1006, 1359, and 1555 cm^{-1} bands are assigned to the trp W18, W17, W16, W7, and W3 vibrations, respectively.[19,20,27−31] The 1179 and 1208 cm^{-1} bands are assigned to the tyr Y9a and Y7a vibrations, respectively.[19,20] The 1613 cm^{-1} band derives mainly from the tyr Y8a vibration, but a small contribution also occurs from the trp W1 band.[19,20] The 932 cm^{-1} band derives from the internal standard perchlorate band. The tyr and trp bands dominate the 229 nm excited t-cyt and h-cyt Raman spectra, because 229 nm excitation occurs within the strong tyr and trp $\pi-\pi^*$ electronic transitions.[17,28,32,33]

Although t-cyt and h-cyt have very similar 3-D protein structures, which consist of single folded polypeptide chains of 104 amino acids,[34,35] they have slightly different amino acid sequences. t-cyt contains two trp residues (trp33 and trp59) and five tyr residues (tyr46, tyr48, tyr67, tyr74, and tyr97), while h-cyt contains only one trp residue (trp59) and four tyr residues (tyr48, tyr67, tyr74, and tyr97).

The difference Raman spectrum in Figure 7, obtained by subtracting the h-cyt spectrum from the t-cyt spectrum, displays the spectrum of the trp33 and tyr46 residues of t-cyt (vide infra). By subtracting the trp59 bands from spectrum of t-cyt, we can obtain the Raman spectrum of the trp33 residue. These trp33 and trp59 residues show different Raman cross sections due to their significantly different environments. For example, the solvent accessible surface area (SASA) of the trp33 is 74 $Å^2$, while that of trp59 is 0 $Å^2$.[15,34,35] Thus, trp59, which is the most conserved residue in the cyt *c* family, is completely buried within the interior of protein, has a totally hydrophobic environment, and has a W18 band Raman cross section of 1.37 barn/(molecule·sr). In contrast, trp33, which is only partially buried, has a decreased Raman cross section of 0.56 barn/(molecule·sr) for the W18 band. Table 2 lists the trp Raman cross sections of these residues.

TABLE 1: Measured λ_{max} and $\tilde{\nu}_{max}$ for the Skatole Electronic Transition to the B_b State and the Cresol Electronic Transition to the L_b State for Various Solvents[a]

	skatole		cresol				
solvent	λ_{max}, nm	$\tilde{\nu}$, cm^{-1}	λ_{max}, nm	$\tilde{\nu}$, cm^{-1}	π^*	α	β
TFE	220.0	45 455	218.0	45 872	0.73	1.51	0.00
water	221.5	45 147	220.0	45 455	1.09	1.17	0.18
heptane	221.1	45 228	220.6	45 331	−0.08	0.00	0.00
acetonitrile	223.0	44 843	222.8	44 883	0.75	0.19	0.31
methanol	223.0	44 843	223.0	44 843	0.60	0.93	0.62
propanol	223.6	44 723	223.8	44 683	0.52	0.78	0.83
hexanol	224.4	44 563	224.2	44 603	0.44	0.75	0.96
ethyl ether	222.9	44 863	224.2	44 603	0.27	0.00	0.47
acetic acid	222.2	45 005	222.5	44 944	0.64	1.12	0

[a] Also listed are solvatochromic parameters of these solvents.[26]

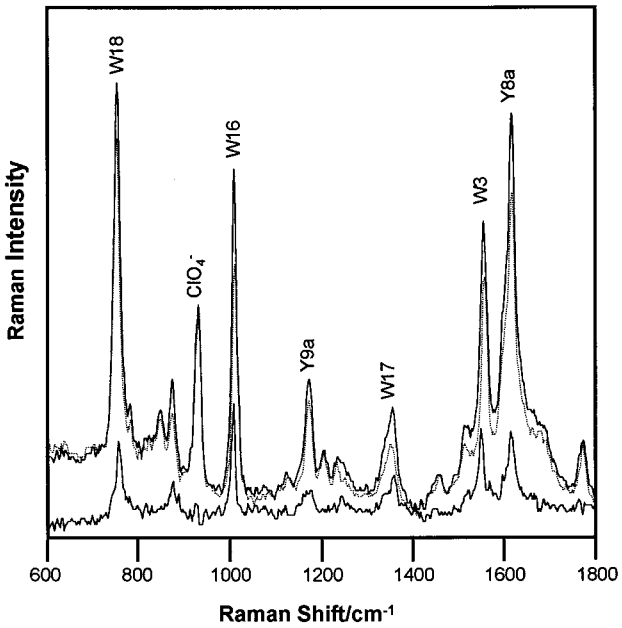

Figure 7. The 229 nm excited resonance Raman spectra of tuna (—) and horse heart (···) cytochrome *c* and their difference spectrum. The concentrations of both tuna and horse heart cytochrome *c* were 41 μM. The 932 cm^{-1} band derives from sodium perchlorate (0.15 M). The Raman difference spectrum is obtained by subtracting the tuna cytochrome *c* Raman spectrum from the horse heart cytochrome *c* Raman spectrum.

TABLE 2: Solvent Accessible Surface Areas and 229 nm Excited Raman Cross Sections of Individual Tryptophan Residues of Tuna Cytochrome *c*

	surface area (Å^2)	σ_{W18} (barn/(molecule·sr))
trp33	74	0.56
trp59	0	1.37

sw-Mb and h-Mb have almost identical 3-D structures but have slightly different amino acid sequences.[36,37] Both sw-Mb and h-Mb contain two trp (trp7 and trp14), while sw-Mb contains three tyr residues (tyr103, tyr146, and tyr151). h-Mb contains only two tyr residues (tyr103 and tyr146). Figure 8 shows the 229 nm excited Raman spectra of sw-Mb (solid line), h-Mb (dashed line), and their difference spectrum obtained by subtracting the h-Mb Raman spectrum from the sw-Mb Raman spectrum. The tyr and trp bands dominate the Mb Raman spectra. The Mb Raman difference spectrum, obtained by subtracting the h-Mb spectrum from the sw-Mb spectrum, shows the Y8a band (1613 cm^{-1}) from the h-Mb tyr151.

Table 3 lists the Raman cross sections and SASAs of the tyr46 in t-cyt and the tyr151 in sw-Mb. Tyr151 with a large SASA of 111 Å^2 has a small Raman cross section of 0.33 barn/(molecule·sr) (Y8a band), while tyr46 with a small SASA of 26 Å^2 has a large Raman cross section of 0.46 barn/(molecule·sr). These results indicate that the 229 nm excited tyr Raman cross sections are also sensitive to their solvent exposure and local environment.

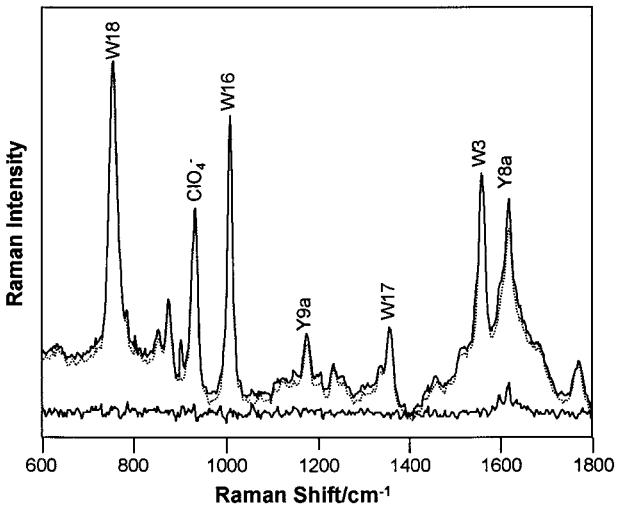

Figure 8. The 229 nm excited resonance Raman spectra of sperm whale (—) and horse heart (···) myoglobin and their difference spectrum. The concentration of sperm whale and horse heart myoglobin was 71 μM. The 932 cm^{-1} band derives from sodium perchlorate (0.15 M). The difference Raman spectrum is obtained by subtracting the sperm whale myoglobin Raman spectrum from the horse heart myoglobin Raman spectrum.

TABLE 3: Solvent Accessible Surface Areas and 229 nm Excited Raman Cross Sections of Individual Tyrosine Residues of Tuna Cytochrome *c* and Sperm Whale Myoglobin

	surface area (Å^2)	σ_{W18} (barn/(molecule·sr))
Cyt tyr46	26	0.44
Mb tyr151	111	0.30

Discussion

Solvent Dependence of Tyr and Trp Electronic Transitions and Raman Cross Sections. Our results demonstrate that both the absorption band maxima and the Raman cross sections of tyr and trp are sensitive to their local environments. The shifts of the tyr and trp ~220 nm electronic absorption maxima depend on solvent solvatochromic properties. Equations 2 and 3 indicate that an increasing solvent hydrogen bond acceptor basicity (β), a decreasing solvent hydrogen bond donor acidity (α), and an increasing solvent polarity and polarizability (π^*) red shift the tyr and trp ~220 nm absorption bands.

TABLE 4: Estimated Relative Peak Shifts ($\Delta\tilde{\nu}_{max}$) for Skatole and Cresol in Amino Acid Residue Solvents and Estimated Solvatochromic Parameters for These Species[26]

amino acid	substitute	π^*	α	β	$\Delta\tilde{\nu}_{max}(s)^a$	$\Delta\tilde{\nu}_{max}(c)^b$
glycine	dimethylformamide	0.88	0.00	0.69	−568	−993
alanine	dimethylacetamide	0.88	0.00	0.69	−568	−993
valine	dihexylacetamide	0.00	0.00	0.77	−474	−968
leucine	dihexylacetamide	0.00	0.00	0.77	−474	−968
isoleucine	dihexylacetamide	0.00	0.00	0.77	−474	−968
methionine	dimethyl sulfoxide	1.00	0.00	0.76	−633	−1065
proline	dimethylacetamide	0.88	0.00	0.76	−614	−1052
phenylalanine	toluene	0.54	0.00	0.11	−138	−467
tryptophan	toluene	0.54	0.00	0.11	−138	−467
serine	methanol	0.60	0.93	0.62	−314	−570
threonine	ethanol	0.54	0.83	0.77	−418	−898
asparagine	ethyl ester	0.55	0.00	0.45	−359	−755
glutamine	butyl ester	0.46	0.00	0.46	−351	−754
tyrosine	benzyl alcohol	0.98	0.00	0.50	−463	−925
cysteine	dimethyl sulfoxide	1.00	0.00	0.76	−633	−1065
lysine	*N*-butylamine	0.00	0.00	0.72	−442	−926
arginine	*N*-butylamine	0.00	0.00	0.72	−442	−926
histidine	pyridine	0.87	0.00	0.64	−535	−950
aspartic acid	acetic acid	0.64	1.12	0.00	−142	−511
glutamic acid	acetic acid	0.64	1.12	0.00	−142	−511

[a] $\Delta\tilde{\nu}_{max}(s) = \tilde{\nu}_{max}$(calculated for skatole in the substituted solvent) $- \tilde{\nu}_{max}$(measured for skatole in water). [b] $\Delta\tilde{\nu}_{max}(c) = \tilde{\nu}_{max}$(calculated for cresol in the substituted solvent) $- \tilde{\nu}_{max}$(measured for cresol in water).

These solvent absorption shifts can be understood by examining the impact of hydrogen bond donation and acceptance on the tyr and trp energy level. When the tyr OH group and the trp NH group act as the hydrogen bond donors, the resulting electron density increases on the oxygen, and nitrogen atoms will increase the energy of the highest occupied molecular orbital (HOMO) of tyr and trp and, thus, red shift the tyr and trp absorption bands. If the tyr OH and the trp NH groups act as proton acceptors, the heteroatom electron densities decrease, and the HOMO energy levels decrease and blue shift the absorption bands.

The results shown in Figures 1 and 4 demonstrate that the bands continuously red shift as the water concentration decreases. The linearity of the shift indicates that the absorption shift results from bulk solvent properties and not from specific hydrogen bonding with solvent molecules.

The tyr and trp environmental Raman cross section dependence derives from the environmental dependence of the absorption spectra. Shifts of the absorption spectra will result in shifts in the Raman excitation profiles. Asher and co-workers previously reported that in aqueous solution the tyr and trp band Raman excitation profile maxima are 2−3 nm red shifted from their absorption maxima.[32,33] The tyr and trp Raman excitation profile maxima are located in the vicinity of 220 nm (depending upon the charge state of the amino and carboxyl groups, which is determined by solution pH). Since 229 nm excitation occurs on the red edge of the Raman excitation profiles, red shifts of these ∼220 nm tyr and trp absorption bands will red shift the Raman excitation profile; this will increase the 229 nm excited tyr and trp Raman cross sections.

Thus, our observed increase in the 229 nm excited tyr and trp Raman cross sections with decreasing water concentrations simply results from absorption and Raman excitation profile red shifts. Thus, 229 nm tyr and trp Raman cross sections will increase for environments with large β and π^* values and a small α value, compared to the case of water.

Protein Environmental Dependence of Tyr and Trp Raman Cross Sections. In proteins the amino acid side-chain environment depends on the local packing of the neighboring side chains, contact with the backbone amide bonds, and the exposure of the residue to the water solvent. An amino acid side chain can be totally buried within the interior of the protein and unavailable to water, or it can be partially buried, with partial exposure to the water solvent. Alternatively, it can be fully exposed to water if it is on the protein exterior. The solvent exposure and accessibility of a residue in a native protein can be quantified by the SASA, which can be easily calculated from the known protein structure by using the algorithm of Lee and Richards.[5]

The position of the tyr and trp absorption maxima and their 229 nm Raman cross sections are determined by the solvatochromic parameters of the surrounding groups. Table 4 tabulates estimated solvatochromic parameters for various amino acid side chains[26] and the absorption shifts compared to water expected for tyr and trp side chains if they were surrounded by these side chains within a protein. We attempted to estimate the solvatochromic parameters for all of the amino acid side chains. Some of these values are gross estimates, since the solvatochromic parameters of even related compounds are, at present, unknown. For these cases we estimated the solvatochromic parameters from values of compounds as close as possible structurally to the amino acid side chain. For small side chains such as glycine, packing against the peptide backbone will occur, and thus we utilized solvatochromic parameters from *N*,*N*-dimethylformamide. For larger side chains we assume little packing against the peptide bond; thus, for phe we utilized the solvatochromic parameters of toluene. Occasionally, we were unable to find structurally similar compounds with known solvatochromic parameters. In this case we selected the most similar compound available. For example, we were forced to use the solvatochromic parameters of a butyl ester as a substitute for asparagine. These compounds and their solvatochromic parameters are tabulated in Table 4. Table 4 also shows that all amino acid side chains red shift the ∼220 nm bands of tyr and trp, compared to water as a solvent. Thus, buried tyr and trp side chains will show larger 229 nm excited Raman cross sections than fully exposed side chains.

Relationship between Tyr and Trp Raman Cross Sections and Absorption Maxima. Figures 9 and 10 show the Raman excitation profiles of the W16 1006 cm^{-1} band of trp (in water, at pH 11.5) and the Y8a 1613 cm^{-1} band of tyr (in water at pH 6.0), as previously measured by our laboratory.[32,33] The solid

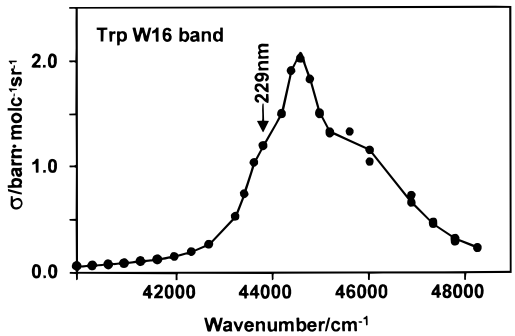

Figure 9. trp W16 band Raman excitation profile in aqueous solution. The dots are the experimental data [Sweeney and Asher, 1990], while the solid curve is a fit by eq 6.

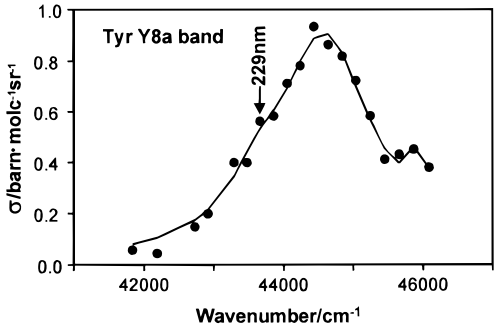

Figure 10. tyr Y8a band Raman excitation profile in aqueous solution. The dots are the experimental data [Ludwig and Asher, 1988], while the solid curve is a fit by eq 8.

lines are phenomenological excitation profile band shapes determined by a fit of the excitation profiles to

$$\sigma = \sum_{i=1}^{3} \frac{a_i}{(\tilde{\nu}_i - \tilde{\nu}_{ex})^2 + \Gamma_i} = \sum_{i=1}^{3} \frac{a_i}{(\tilde{\nu}_{H_2O} - \Delta\tilde{\nu} - \tilde{\nu}_{ex})^2 + \Gamma_i} \quad (4)$$

where σ is the trp or tyr Raman cross section (barn/(molecule·sr)), $\tilde{\nu}_i = \tilde{\nu}_{H_2O} - \Delta\tilde{\nu}$, where $\tilde{\nu}_{H_2O}$ is the frequency of the tyr or trp absorption band maximum in water and $\Delta\tilde{\nu}$ is the absorption band (and excitation profile) solvent shift for a particular tyr or trp residue in its environment compared to that in water. ν_{ex} is the Raman excitation frequency. a_i and Γ_i are the fitting constants.

The Raman excitation profiles show some vibronic substructure, which are well fit to the sum of three Lorentzians as shown in Figures 9 and 10. The values $\tilde{\nu}_i$ specify the central frequency of the individual Lorentzian components of the Raman excitation profile. Our solvent composition studies showed essentially no solvent dependence of the maximum molar absorptivities and the absorption band shapes. The only impact of changes in solvent was shifts of the entire absorption band. For nonblocked trp the position of the absorption also depends on solution pH, because there are ~2 nm shifts between the zwitterionic form and the cation and anion forms. Essentially, we observe no band shape changes, with only slight molar absorptivity changes. Since the absorption band shapes and excitation profiles are little changed by environment, we expect that the Raman excitation profiles will rigidly shift as absorption band shifts. Thus, we calculate the excitation profiles of tyr and trp in different environments by rigidly shifting our previously measured Raman excitation profiles (Figures 9 and 10) identically with shifts in the ~220 nm absorption bands.

The band shape of the W16 trp (pH 11.5) Raman excitation profile is well fit to the following sum of three Lorentzians as demonstrated by the solid curve in Figure 9.[32]

$$\sigma^{b}_{w16}(\Delta\tilde{\nu},\tilde{\nu}_{ex}) = \frac{67900}{(43767 - \Delta\tilde{\nu} - \tilde{\nu}_{ex})^2 + 122900} + \frac{336900}{(44606 - \Delta\tilde{\nu} - \tilde{\nu}_{ex})^2 + 214900} + \frac{1367000}{(45933 - \Delta\tilde{\nu} - \tilde{\nu}_{ex})^2 + 1339000} \quad (5)$$

where $\sigma^{b}_{w16}(\Delta\tilde{\nu},\tilde{\nu}_{ex})$ is Raman cross sections of the 1006 cm^{-1} W16 trp band in water at pH 11.5.

The UV absorption spectra of zwitterionic trp at pH 7.0 is blue shifted by 2.2 nm or 450 cm^{-1} compared to anionic trp at pH 11.5, while the blocked trp is blue shifted 1.5 nm (310 cm^{-1}) compared to anionic trp at pH 11.5. All of these trp solutions show essentially identical band shapes and molar absorptivities. Thus, the W16 trp (pH 7.0) band Raman excitation profile for a neutral trp side chain (modeled as our blocked trp) is given by

$$\sigma_{w16}(\Delta\tilde{\nu},\tilde{\nu}_{ex}) = \frac{67900}{(44077 - \Delta\tilde{\nu} - \tilde{\nu}_{ex})^2 + 122900} + \frac{336900}{(44916 - \Delta\tilde{\nu} - \tilde{\nu}_{ex})^2 + 214900} + \frac{1367000}{(46243 - \Delta\tilde{\nu} - \tilde{\nu}_{ex})^2 + 1339000} \quad (6)$$

As demonstrated by the solid curve in Figure 10, the band shape of the pH 7 Y8a tyr 1613 cm^{-1} band Raman excitation profile is well fit to[33]

$$\sigma^{0}_{Y8a}(\Delta\tilde{\nu},\tilde{\nu}_{ex}) = \frac{32380}{(43626 - \Delta\tilde{\nu} - \tilde{\nu}_{ex})^2 + 221800} + \frac{594500}{(44598 - \Delta\tilde{\nu} - \tilde{\nu}_{ex})^2 + 675700} + \frac{7250}{(45963 - \Delta\tilde{\nu} - \tilde{\nu}_{ex})^2 + 28900} \quad (7)$$

while that of the blocked tyr is blue shifted by 0.8 nm (160 cm^{-1}) and is given by

$$\sigma_{Y8a}(\Delta\tilde{\nu},\tilde{\nu}_{ex}) = \frac{32380}{(43786 - \Delta\tilde{\nu} - \tilde{\nu}_{ex})^2 + 221800} + \frac{594500}{(44758 - \Delta\tilde{\nu} - \tilde{\nu}_{ex})^2 + 675700} + \frac{7250}{(46123 - \Delta\tilde{\nu} - \tilde{\nu}_{ex})^2 + 28900} \quad (8)$$

These expressions can be utilized to correlate observed changes in absolute Raman cross sections to Raman excitation profile shifts and, thus, to absorption band shifts. Table 5 compares the measured and calculated absorption shifts for ac-trp-ee as a function of solvent composition and the measured and calculated (eq 6) trp Raman cross sections. The excellent agreement between the calculated and observed results is clearly evident from the calculated points shown in Figure 3.

Table 6 compares the measured and calculated absorption shifts measured for ac-tyr-ee as a function of solvent composition and the measured and calculated (eq 8) tyr Raman cross sections in the water−propanol solvent mixtures. These

TABLE 5: Measured and Calculated Absorption Peak Shifts versus Water (~220 nm Trp) and Trp Raman Cross Sections of ac-trp-ee in Water−Propanol Solvent Mixtures[a]

	water (%)				
	100	75	50	25	0
measured $\Delta\tilde{\nu}$ (cm^{-1})	0	106	212	318	424
calculated $\Delta\tilde{\nu}$ (cm^{-1})	0	98	196	294	392
σ_{cal} (barn/(molecule·sr))	0.60	0.72	0.88	1.04	1.16
σ_m (barn/(molecule·sr))	0.52	0.78	0.92	1.00	1.15

[a] σ_{cal} is the calculated 229 nm excited trp W16 band Raman cross section of ac-trp-ee in water−propanol solvent mixture by using eq 6 and absorption profile. σ_m is the measured 229 nm excited trp W16 band Raman cross section of ac-trp-ee in the water−propanol solvent mixture.

TABLE 6: Measured and Calculated Absorption Peak Shifts versus Water (~220 nm Tyr) and Measured Tyr Raman Cross Sections of ac-tyr-ee in Water−Propanol Solvent Mixtures[a]

	water (%)				
	100	75	50	25	0
measured $\Delta\tilde{\nu}$ (cm^{-1})	0	193	386	579	772
calculated $\Delta\tilde{\nu}$ (cm^{-1})	0	158	315	473	630
σ_{cal} (barn/(molecule·sr))	0.46	0.55	0.62	0.71	0.82
σ_m (barn/(molecule·sr))	0.38	0.46	0.49	0.54	0.56

[a] σ_{cal} is the calculated 229 nm excited tyr Y8a band Raman cross section of ac-tyr-ee in water−propanol solvent mixtures by using eq 8 and absorption profile. σ_m is the measured 229 nm excited tyr Y8a band Raman cross section of ac-tyr-ee in water−propanol solvent mixtures.

calculated data are also displayed in Figure 6. Although the calculated tyr cross sections are ~40% larger than those observed, almost identical slopes are observed for the cross section increases with increasing propanol concentrations.

The 229 nm excited trp Raman cross sections are more sensitive to environmental changes due to the larger slope of the trp Raman excitation profiles with frequency, compared to the case of tyr. These results demonstrate that we can use the Raman cross sections to monitor the environments of tyr and trp for different Raman excitation wavelengths between 217 and 240 nm.

Tyr and Trp Residue Environments in Proteins. We can estimate the effective solvatochromic parameters of the tyr and trp environments in a protein by averaging the solvatochromic parameters of the surrounding residues and by accounting for the water exposure of the tyr and trp. The total surface area of tyr and trp residues is 187 and 217 Å^2, respectively.[34] For example, h-cyt trp59 is totally buried inside the protein (SASA is 0 Å^2) and is surrounded by leu35, arg38, lys39, gly41, gln42, lys60, glu61, glu62, thr63, glu66, tyr67, lys73, tyr74, and the heme.[35] We estimate that the average solvatochromic parameter of the trp59 environment has a π-scale value of 0.44, an α-scale value of 0.32, and a β-scale value of 0.51. This would result in a solvent shift $\Delta\tilde{\nu}$ of 320 cm^{-1} for the trp absorption and excitation profile, which would result in a calculated trp59 W16 Raman cross section of 1.05 barn/(molecule·str), which is within 23% of the measured Raman cross section of 1.37 barn/(molecule·str).

The t-cyt trp59 is also totally buried and is surrounded by leu35, arg38, lys39, gly41, gln42, *asn60*, *asn61*, *asp62*, thr63, glu66, tyr67, lys73, tyr74, and the heme.[36] The lys60, glu61, and glu62 around the h-cyt are replaced by *asn60*, *asn61*, and *asp62* residues for t-cyt trp59. These two sets of residues have very similar effective solvatochromic parameters since it is the methylene groups of these side chains that are adjacent to the trp59. Thus, the two trp59 residues are expected to have the same environmental solvatochromic parameters and identical Raman cross sections.

The h-cyt trp33 is partially buried (SASA is 74 Å^2) and is surrounded by val20, glu21, asn22, gly23, lys25, his26, leu30, gly34, asn60, ala101, and ser103. For the surrounding amino acids we estimate an average solvatochromic parameter π-scale value of 0.53, an α-scale value of 0.19, and a β-scale value of 0.59. We average this with the solvatochromic parameters of water given that this residue has an SASA of 74 Å^2 out of its total surface area of 217 Å^2.[34] We calculate a resultant trp33 W16 Raman cross section of 0.97 barn/(molecule·str), compared to our measured Raman cross section of 0.56 barn/(molecule·str). This large difference between the calculated and measured Raman cross sections of trp33 could result from more exposure of the near surface trp33 residue to water in the solution phase than occurs in the solid crystal state measured by X-ray diffraction. This argument is strengthened by our previous observations that the Raman cross sections of the trp in h-Mb decrease to values indicating full solvent exposure when the protein is unfolded and the trp become fully exposed.[20]

h-cyt has four tyr, while t-cyt has five tyr. Each of the three tyr67, tyr74, and tyr97 residues of t-cyt and h-cyt have identical surrounding residues.[35,36] In addition, the side-chain groups in closest proximity to tyr48 are very similar. For example, the phe46 and thr47 residues that are close to tyr48 in h-cyt are replaced by tyr47 and ser47 in t-cyt. Thus, tyr48, tyr67, tyr74, and tyr97 should have similar Raman cross sections in t-cyt and h-cyt. Thus, if we subtract the spectrum of h-cyt from t-cyt, we will expose the spectrum of the t-cyt tyr 46.

The t-cyt tyr46 is largely buried (SASA is 26 Å^2) and is surrounded by val26, lys27, gly29, glu44, gly45, ser47, tyr48, and lys79. The calculated tyr Y8a Raman cross section is 0.76 barn/(molecule·sr), while the measured Raman cross section is 0.44 barn/(molecule·sr). This is 73% larger, which indicates a lack of accuracy of our model in this case.

sw-Mb has three tyr while h-Mb has two tyrosines.[37,38] The two identical tyr103 and tyr146 residues of sw-Mb and h-Mb have essentially identical environments and Raman cross sections. Thus, the myoglobin difference spectrum displays the sw-Mb tyr151 Raman spectrum. The sw-Mb tyr151 is mostly exposed to water (SASA is 111 Å^2) and is adjacent to thr95, lys98, ile99, lys102, pro100, ala143, lys147, leu149, gly150, gln152, and gly152. We calculate that the tyr151 Y8a Raman cross section is 0.62 barn/(molecule·sr), which again is about 2-fold larger than the measured Raman cross section of 0.30 barn/(molecule·sr).

Our model appears to accurately give the trp Raman cross sections but systematically overestimates the tyr cross sections. The tyr discrepancies between the measured and calculated tyr Raman cross sections in proteins may be due to poor modeling of the solvatochromic parameters. For example, the α parameter, which is more important for tyr than trp, is estimated to be zero for most amino acid side chains. Obviously, we must improve the solvatochromic parameters used in Table 4. Nonetheless, both the measured and calculated individual 229 nm excited tyr and trp Raman cross sections are excellent probes of environmental changes around the tyr and trp residues.

We can use these results to correlate the solvent exposed surface area to the Raman cross section of the trp W16 band and the tyr Y8a band. Figure 11 shows a calculated plot of the 229 nm Raman cross sections of these bands for the tyr and trp residues as a function of solvent accessibility. We assume for this calculation that the buried residue is surrounded by aliphatic

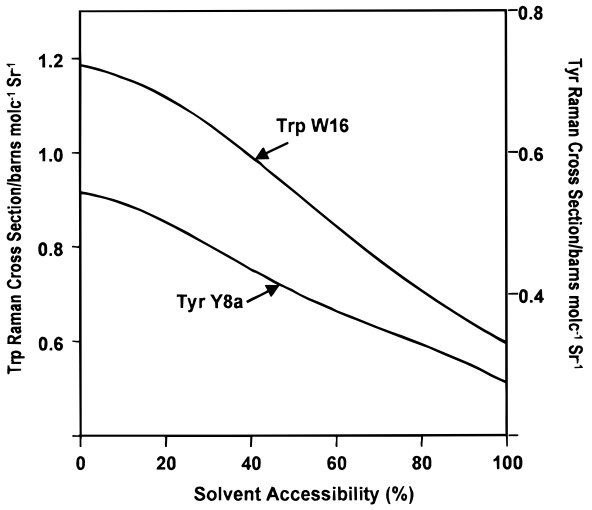

Figure 11. Calculated dependence of the Raman cross sections of trp W16 and tyr Y8a bands on the solvent accessibility, assuming these buried residues are surrounded by valines. The estimated relative peak shifts ($\Delta\tilde{\nu}_{max}$) are calculated from the solvatochromic parameters for valine in Table 4. The plots for tyr and trp are calculated by eqs 6 and 8, respectively.

groups with solvatochromic parameters identical to those of valine (Table 4). We have multiplied our tyr Raman cross section data by 0.6 to make them conform to the experimental results discussed above. This plot allows one to easily calculate the increase in water exposure from change in the observed Raman cross sections.

Trp W7 Marker Band. The bandwidth of the trp W7 1363 cm^{-1} band, which involves N_1C_8 stretching of the indole ring, was previously correlated with the hydrophilicity of the trp environment in proteins. A narrow and intense 1363 cm^{-1} band was thought to be indicative of a buried trp.[31] Our water−propanol results are not consistent with this simple picture. Although the band contour changes somewhat between 100% and 75% water, little further change occurs as the solvent becomes more hydrophobic as it approaches 100% propanol (Figure 2). Both trp59 and trp33 of cyt *c* display a narrow and strong W7 band, while ac-trp-ee displays a broad band in solution. For example, the 1363 cm^{-1} band bandwidth of trp (20 cm^{-1}) in water−propanol solvent mixture is ca. 50% broader that that in cyt (14 cm^{-1}). It is likely that the narrowing results not from environmental hydrophobicity but is a result of a decrease in the inhomogeneous line width of this Raman band.

Part of the width of the W7 band results from the fact that it is a Fermi doublet,[27] with features at 1360 and 1340 cm^{-1}, which derive from Fermi resonance between an N_1C_8 stretching mode and the overtone of an out-of-plane bending vibration.[27] Our results agree with those previous studies; the trp I_{1360}/I_{1340} ratio decreases with increasing water composition.

Conclusion

Our studies on tyr and trp model compounds in various solvents demonstrate that the ~220 nm electronic absorption band maxima red shift upon an increase of hydrogen bond donor basicity, upon a decrease of hydrogen bond acceptor acidity, or upon an increase of polarity of solvent environment. We have examined both the absorption and Raman spectra of ac-trp-ee and ac-tyr-ee in water−propanol solvent mixtures and find that the 229 nm excited tyr and trp Raman cross sections increase with decreasing water composition due to red shifts of the ~220 nm absorption bands. The 229 nm excited tyr and trp protein Raman cross sections are sensitive to their solvent accessible surface areas; the smaller the surface area, the larger the Raman cross section. We derive relationships between the Raman cross sections and the solvent accessible surface areas. Our results show that tyr and trp can be utilized as intrinsic probes to monitor the protein local environments around the tyr and trp residues.

Acknowledgment. We gratefully acknowledge support from NIH Grant R01GM30741. We also thank Drs. Kevin Willis and Arthur Szabo for generously providing the sperm whale myoglobin sample.

References and Notes

(1) Dill, K. A.; Chan, H. S. *Nature Struct. Biol.* **1997**, *4*, 10.
(2) Fischer, D.; Rice, D.; Bowte, J. U.; Eisenberg, D. *Faseb J.* **1995**, *10*, 126.
(3) Thornton, J. M.; Jones, D. T.; MacArthur, M. W.; Orengo, C. M.; Swindells, M. B. *Philos. Trans. R. Soc. London B* **1995**, *348*, 71.
(4) Kim, P. S.; Baldwin, R. L. *Annu. Rev. Biochem.* **1990**, *59*, 631.
(5) Lee, B.; Richards, F. M. *J. Mol. Biol.* **1971**, *55*, 379.
(6) Connolly, M. L. *Science* **1983**, *221*, 709.
(7) Richards, F. M.; Lim, W. A. *Q. Rev. Biophys.* **1994**, *26*, 423.
(8) Richards, F. M. *Annu. Rev. Biophys. Bioeng.* **1977**, *6*, 151.
(9) Richmond, T. J. *J. Mol. Biol.* **1984**, *178*, 63.
(10) Richards, F. M. *Methods Enzymol.* **1985**, *115*, 440.
(11) Platt, J. R. *J. Chem. Phys.* **1949**, *17*, 484.
(12) Nemethy, G.; Ray, A. *J. Phys. Chem.* **1973**, *77*, 64.
(13) Demchenko, A. P. *Ultraviolet Spectroscopy of Proteins*; Springer-Verlag: Berlin, 1986; pp 1−63.
(14) Woody, R. W.; Dunker, A. K. *Circular Dichroism and the Conformational Analysis of Biomolecules*; Fasman, G. D., Ed.; Plenum Press: New York, 1996; pp 109−157.
(15) Eftink, M. R. *Methods Biochem. Anal.* **1991**, *35*, 127.
(16) Johnson, C. R.; Ludwig, M. L.; O'Donnell, S.; Asher, S. A. *J. Am. Chem. Soc.* **1984**, *106*, 5008.
(17) Asher, S. A.; Ludwig, M. L.; Johnson, C. R. *J. Am. Chem. Soc.* **1986**, *108*, 3186.
(18) Rodgers, K. R.; Su, C.; Subramaniam, S.; Spiro, T. G. *J. Am. Chem. Soc.* **1992**, *114*, 3697.
(19) Cho, N.; Song, S.; Asher, S. A. *Biochemistry* **1994**, *33*, 5932.
(20) Chi, Z.; Asher, S. A. *Biochemistry* **1998**, *37*, 2865.
(21) Hu, X.; Spiro, T. G. *Biochemistry* **1997**, *36*, 15701.
(22) Dudik, J. M.; Johnson, C. R.; Asher, S. A. *J. Chem. Phys.* **1985**, *82*, 1732.
(23) Asher, S. A.; Johnson, C. R.; Murtaugh, J. *Rev. Sci. Instrum.* **1983**, *54*, 1657.
(24) Asher, S. A.; Chi, Z. S. A. *NATO ASI Series Volume, Biomolecular Structure and Dynamics: Recent Experimental and Theoretical Advances*; Vergoten, G., Ed.; Kluwer Academic Publishers: Dordrecht, 1997; pp 263.
(25) Asher, S. A.; Bormett, R. W.; Chen, X. G.; Lemmon, D. H.; Cho, N.; Peterson, P.; Arrigoni, M.; Spinelli, M.; Cannon, J. *Appl. Spectrosc.* **1993**, *47*, 628.
(26) Kamlet, M. J.; Abboud, G. L. M.; Taft, R. W. *Prog. Phys. Org. Chem.* **1981**, *13*, 485.
(27) Harada, I.; Takeuchi, H. *Spectroscopy of Biological Systems*; Clark, R. J. H., Hester, R. E., Eds.; John Wiley and Sons: New York, 1986; pp 113−176.
(28) Johnson, C. R.; Ludwig, M. L.; Asher, S. A. *J. Am. Chem. Soc.* **1986**, *108*, 905.
(29) Asher, S. A.; Larkin, P. J.; Teraoka, J. *Biochemistry* **1994**, *30*, 5944.
(30) Miura, T.; Takeuchi, H.; Harada, I. *J. Raman Spectrosc.* **1989**, *20*, 667.
(31) Sweeney, J. A.; Harmon, P. A.; Asher, S. A.; Hutnik, C. M.; Szabo, A. G. *J. Phys. Chem.* **1991**, *95*, 7531.
(32) Sweeney, J. A.; Asher, S. A. *J. Phys. Chem.* **1990**, *94*, 4784.
(33) Ludwig, M. L.; Asher, S. A. *J. Am. Chem. Soc.* **1988**, *110*, 1005.
(34) Miller, S.; Janin, J.; Lesk, A. M.; Chothia, C. *J. Mol. Biol.* **1987**, *196*, 641.
(35) Bushnell, G. W.; Louie, G. V.; Brayer, G. D. *J. Mol. Biol.* **1990**, *214*, 585.
(36) Swanson, R.; Trus, B. L.; Mandel, N.; Mandel, G.; Kallai, O. B.; Dickerson, R. E. *J. Biol. Chem.* **1977**, *252*, 759.
(37) Evans, S. V.; Brayer, G. D. *J. Biol. Chem.* **1983**, *263*, 4263−4268.
(38) Philips, S. E. V. *J. Mol. Biol.* **1980**, *142*, 531.